Reducing Complexity, Enhancing Precision: Predicting Compliant Surface Transitions in Walking via Neighborhood Component Analysis

Charikleia Angelidou and Panagiotis Artemiadis*, IEEE Senior Member

Abstract— Achieving volitional control for powered prostheses necessitates reliable sensing modalities capable of accurately interpreting user intentions to walk, run, and transition on and between surfaces of varying compliance. However, the optimal amount of information and signal sources that can be used as input to such strategies is vet a question to be determined. In this work, we are building upon the foundations of our prior studies and focusing on reducing the number of sensors and recorded signals needed to reliably predict and classify user intent to transition from rigid to compliant surfaces of variable stiffness. Comparing two feature selection and dimensionality reduction approaches, we show that the feature vectors generated by the Neighborhood Component Analysis (NCA) algorithm exceed the prediction accuracy capabilities of Particle Swarm Optimization (PSO) by up to 15%, while NCA reduces the number of the selected classification input features by 91% on average. Employing a k Nearest Neighbors classification framework in conjunction with a Naive Bayes approach, our algorithm can achieve an average predictive accuracy of 77.25%, leading to reliable predictions about the upcoming steps of the user.

I. INTRODUCTION

In order for individuals with lower limb amputation to regain mobility and achieve natural, intuitive locomotion, it is necessary to develop predictive models capable of understanding complex movements and mode transitions, particularly on surfaces of varying stiffness [1]. A critical aspect of these models lies in the sensors employed to capture the intricate interplay of leg and body dynamics with the environment. Sensors that measure the muscle activity and kinematics of the wearer are usually employed to capture the perception and proactive actions of the wearer, as well as monitor the reactive responses evoked by various environmental stimuli. However, as the pursuit of precision and accuracy in predicting surface compliance transitions continues, a need arises to reevaluate the number and types of sensors utilized. For individuals with lower limb amputation specifically, the added weight, complexity, and maintenance requirements of multiple sensors suggested for most conventional approaches can hinder the adoption and long-term use of prosthetic and assistive devices [2].

Researchers have suggested employing high-level control strategies for online classification of the user's intended ambulation mode, which commonly rely on onboard mechanical sensors, such as inertial measurement units (IMU)

and load cells [3,4], or a combination of mechanical sensors along with muscle activity signals, such as electromyography (EMG) [5,6], or sonomyography [7,8]. The integration of vision and depth sensing has also shown improvements in environment and ambulation mode classification [9]. While these studies demonstrate high accuracy levels, flawless classification in the realm of compliant surfaces and transitions between terrains of variable stiffness remains elusive. Recent works [10, 11] have advanced the current knowledge on prediction systems for compliant terrain; however, experience has shown that increasing the number of recorded signal sources - thus increasing the level of system complexity - does not necessarily yield analogously high performance.

In light of these challenges, there is an ongoing quest for enhancing locomotion prediction tasks for individuals with lower limb amputation while employing a minimal sensor approach. By strategically selecting and fusing a minimal number of sensors, we can develop efficient predictive models that balance accuracy with practicality. This study therefore aims to assess the effectiveness of various suggested data sources for user intent recognition and identify a concise set of informative sources for high-level prosthetic ankle control. Building upon our previous works [10, 11], we explore and compare the efficiency of two feature selection algorithms in determining a reduced set of data inputs, ensuring accurate intent recognition when transitioning between surfaces of more than one level of stiffness for the case of compliant terrains. Specifically, we explore the integration of EMG, kinematic signals, and Ground Reaction Forces (GRFs), aiming to streamline the predictive modeling process. We endeavor to create a framework that does not only accurately predict transitions to compliant surfaces but does so with minimal intrusiveness. Our objective is to advance the existing knowledge regarding anticipatory mechanisms during transitions to compliant surfaces and broaden the relevance of our research to encompass various surfaces encountered in activities of daily living (ADLs).

II. METHODS

A. Participants

This analysis includes results from 5 healthy, able-bodied (AB) participants (3 males, 2 females) with an average age of 26.2 ± 1.1 years. Each participant provided written consent to complete a series of walking trials on a unique robotic treadmill following a pre-defined experimental protocol. The experimental protocol was approved by the University of Delaware Institutional Review Board (IRB ID# 1544521-7).

^{*}This material is based upon work supported by the National Science Foundation under Grants No. 2020009, 2015786, 2025797, and 2018905.

Charikleia Angelidou and Panagiotis Artemiadis are with the Mechanical Engineering Department, at the University of Delaware, Newark, DE 19716, USA. cangelid@udel.edu, partem@udel.edu

^{*}Corrresponding author

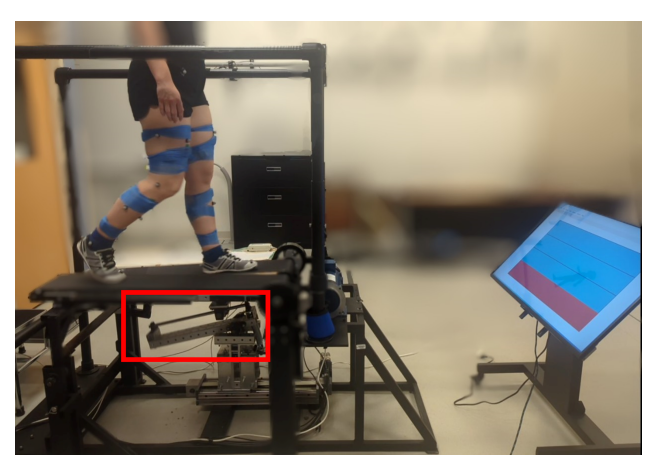


Fig. 1: VST and visual feedback setup. The subject is walking on a low stiffness surface (red patch) preparing to step back on a rigid surface (blue patch).

B. Experimental Setup & Protocol

All participants completed a series of 5-minute long walking trials on the Variable Stiffness Treadmill (VST), a robotic split-belt platform that allows the alteration of the vertical compliance of the left belt as desired [12, 13]. This unique setup allows us to conduct in-lab experiments and simulate walking scenarios on compliant surfaces that correspond to ADLs.

Using the VST, the rigid (R) ground in terms of stiffness is modeled as 1 MN/m, while the compliant ground for this series of experiments was modeled between $20 \, kN/m$ and $110 \, kN/m$. The compliant stiffness range was further separated into three distinct levels that correspond to scenarios of high (H, e.g., thick carpet), medium (M, e.g., grass), and low stiffness (L, e.g., sand) (see Table I). To achieve a similar belt displacement for all participants, the stiffness at which each subject walked was determined as their body weight measurement divided by the desired belt deflection (d) for each level. Throughout the entire experimental session, participants were required to wear a body weight support harness, which did not counterbalance any of the subject's weight and was solely employed for safety purposes.

	S_R	S_H	S_M	S_L
Upper Bound (kN/m)	1000	110	69	39
Lower Bound (kN/m)	1000	70	40	20
Belt Deflection d (cm)	0	1	2	3

TABLE I: Stiffness ranges of each tested condition (R, H, M, and L) and their corresponding left belt deflection (d).

To familiarize the participants with the VST, we included a training phase during which no data were recorded. The training session served the exclusive purpose of acclimating the participants to the variable stiffness settings of our treadmill, introducing them to a new visual feedback setup, as well as self-selecting a comfortable walking speed that would remain fixed throughout the actual walking trials. After selecting a uniform treadmill speed value of $0.90 \ m/s$ and completing the training phase, all participants engaged

in the evaluation trials. The data analyzed throughout this work pertains to data collected during the evaluation trials.

The experimental protocol consisted of walking on the VST, while both treadmill belts were set to rigid. At regular intervals of about three to five consecutive gait cycles, expected, unilateral (left belt) stiffness perturbations of a prespecified stiffness level $(S_H,\,S_M,\,{\rm or}\,S_L)$ would occur for the duration of a full gait cycle, before returning to the rigid setting. For reference purposes, in this work, a gait cycle is defined as starting and ending at left heel strike. The right belt was set to rigid (S_R) at all times. Each trial was followed by a 1-minute long break before progressing to the remaining stiffness levels. The order of the conditions tested in each trial was randomized across participants.

As outlined above, all perturbations were anticipated, and the participants were visually informed of the upcoming surface stiffness change three gait cycles before it occurred. The visual feedback setup included a large monitor that was placed in front of the treadmill at a comfortable height for the subject to see it while walking (see Fig. 1). The visual feedback consisted of a colored patch (green for H, yellow for M, red for L, and blue for R) that would travel from the top to the bottom of the screen at each completed gait cycle. The bottom of the screen aligned with the participant's current left step; thus, when the bottom of the screen was blue the left belt setting was R, but when the bottom of the screen changed color (green, yellow, or red) the left belt setting was set to S_H , S_M , or S_L respectively (see Fig. 1). Since our strategy depends on the anticipatory mechanisms in human locomotion, it is important to emphasize that the data analysis focuses on the gait cycles preceding each perturbation, which are then compared with all R gait cycles, except for the single R gait cycles following each surface stiffness change.

C. Data Collection

Throughout the evaluation trials, we collected EMG signals from the muscles of both the left and right legs. EMG wireless sensors (Trigno, Delsys Inc.) were strategically placed on specific muscles, including the tibialis anterior (TA), soleus (SOL), gastrocnemius (GA), rectus femoris (RF), vastus medialis (VM), vastus lateralis (VL), and biceps femoris (BF). The muscles of the left limb will hereon be marked with an L ahead of the muscle name (i.e., LTA), while the muscles of the right limb will hereon be marked with an R ahead of the muscle name (i.e., RTA). The muscle locations were determined following SENIAM recommendations [14], and the EMG signals were sampled at 2 kHz. Lower-body kinematics were additionally collected using 20 reflective markers placed on the pelvis, thighs, shanks, and feet of the subjects. Kinematic data was sampled at 100 Hz using a VICON motion capture system integrated with the VST implementations [15]. The full subject instrumentation is also schematically presented in Fig. 2. Finally, ground reaction forces (GRF) under the leading (left) foot were recorded at a 65Hz sampling rate using high-resolution force mats (Tekscan 3,510 Medical Sensors) inserted between

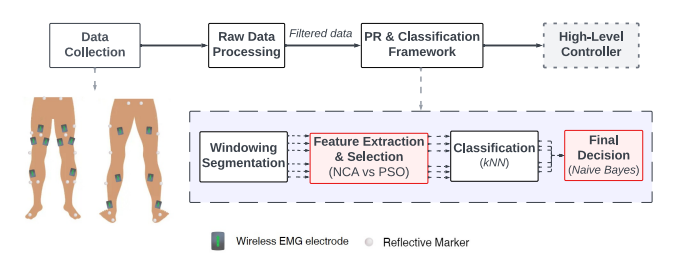


Fig. 2: Overview of the proposed research framework. The blocks marked in red are modifications to our existing framework that we explore in this study. The blocks marked in black are analyzed in detail in our previous works [10, 11].

the belt and the treadmill supporting platform. In total, 35 sources of information (14 EMG, 20 kinematic, 1 GRF) were utilized.

The raw kinematic and EMG data were synchronized by applying a robust kinematic algorithm for heel-strike detection [16]. Force mat data were synchronized with motion capture and EMG data using a trigger signal from VICON Nexus. For each subject, outlier gait cycles were detected using a systematic outlier detection method [17].

D. Data Analysis

The framework employed in this study is based on our previous works [10, 11], where we developed a pattern recognition (PR) and classification algorithm for predicting transitions to compliant surfaces. Compared to our previous works, this paper focuses on exploring different signal sources as inputs to the proposed algorithm, juxtaposing it with an alternative feature selection methodology especially tailored to the needs of the k-Nearest Neighbor (kNN) classification. The schematic representation of the modified proposed framework is depicted in Fig. 2.

- and kinematic data of each gait cycle were segmented into 50% overlapping windows of 150ms. The window partitioning was exclusively applied to the data between Left Toe-Off (LTO) and Left Heel-Strike (LHS), resulting in a total of six analysis windows per gait cycle. The goal we are trying to achieve by employing a window segmentation technique is to derive a prompt decision about the user's next step depending on gait cycle history information up until a few milliseconds before the LHS on the compliant surface.
- 2) Feature Extraction: The EMG features extracted from each muscle per window and per gait cycle included the Mean Absolute Value, Waveform Length, Difference Variance Value, Root Mean Square, Simple Square Integrated, Integrated EMG, Variance of EMG, Difference Absolute Mean Value, Standard Deviation, Average Amplitude Change, Kurtosis, and Skewness [10]. The above features constitute a non-exhaustive list of myoelectric signal features employed in pattern recognition for prosthetic control. A new addition to the existing pool of features is the incorporation of 6th-order Autoregressive model coefficients which correspond to 6 new features. The AR coefficients characterize each sample in the EMG signal as a linear combination of its preceding samples as shown below:

$$x_k = \sum_{i=1}^{N} a_i x_{k-i} + W_k \tag{1}$$

, where x_k represents the pre-processed EMG signal sample at discrete time $k=0,1,2,\ldots,K$, with K as the number of samples in a specific segment. N is the order of the AR model with a_i coefficients, and W_k is white noise [18].

The kinematic variables utilized for this study included the left and right hip, knee, and ankle flexion angles (LHF, LKF, LAF, and RHF, RKF, RAF respectively), the left and right knee and ankle angular velocity (LKV, LAV, RKV, RAV respectively), and acceleration (LKA, LAA, RKA, RAA respectively), as well as the center of mass translation in the x, y, and z coordinates (CoM_x , CoM_y , CoM_z). The features extracted from each kinematic variable included the maximum, mean, and minimum of the corresponding values within each segmented window. The CoM was estimated as the average between the 4 pelvis markers (see Fig. 2).

Finally, we concatenated the EMG and kinematic features of each window to a final feature vector of 303 features per window per gait cycle (EMG: 14 muscles × 18 features = 252 features/ window; Kinematics: 17 variables \times 3 features = 51 features). The resulting feature vectors were then extended by the concatenation of three additional GRF features. These features included the 1st GRF peak (passive peak corresponding to weight acceptance), and the 2nd GRF peak (active peak during push-off) [19]. In between these peaks, as the subject weight is distributed from heel to toe, there is a valley area that is formed, the minimum of which corresponds to the third GRF feature extracted. These three features were calculated as stand-alone features between the right and left toe-off gait events of each gait cycle and were subsequently added to each existing feature vector, expanding the total number of features to 306.

3) Feature Selection with Neighborhood Component Analysis (NCA) vs Particle Swarm Optimization (PSO): To retain the crucial features of the dataset while reducing system complexity we turned our attention to an appropriate feature selection method that would enable us to choose a subset of pertinent features for incorporation into our classification model, facilitating faster and more accurate predictions. Our previous work concentrated on Particle Swarm Optimization (PSO) for feature extraction. The PSO implementation and parameters are analyzed in detail in [10].

For this study, we explored further alternatives for the feature selection component. We specifically opted for the Neighborhood Component Analysis (NCA) algorithm. The implementation of the algorithm was completed in Matlab with the built-in function fscnca. Considering the multiclass classification problem at hand, we separated the data into 70% training and 30% testing sets containing n observations, which, in our case, correspond to gait cycles. The training set is defined as $S = \{(x_i, y_i), i = 1, 2, \ldots, n\}$, where $x_i \in \mathbb{R}^p$ are the feature vectors and $y_i \in \{R, H, M, L\}$ are the class labels. The aim here is to learn a classifier $f: \mathbb{R}^p \to \{R, H, M, L\}$ that accepts a feature vector and makes a prediction f(x) for the true label y. The

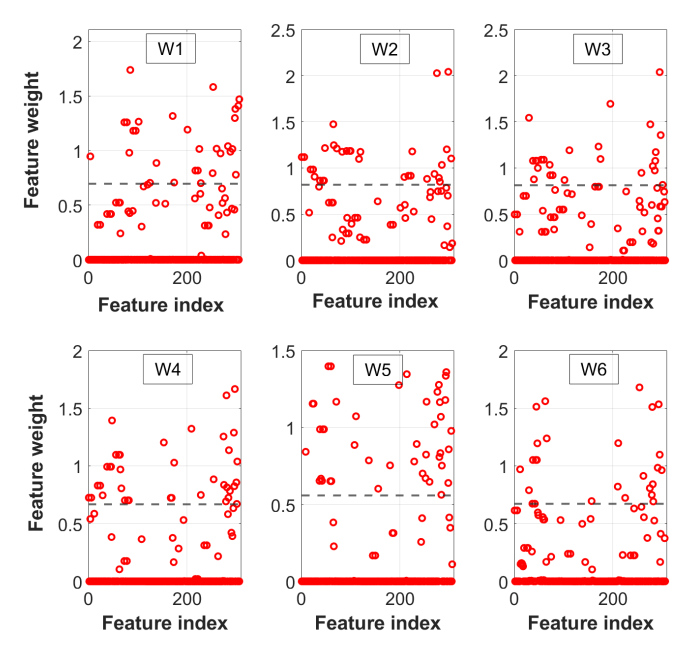


Fig. 3: NCA generated feature weights for representative subject data. Each red circle corresponds to the feature weight assigned to each of the 306 extracted features per window. The grey dashed line represents the weight threshold that the features need to abide by to be selected by NCA.

feature weight (FW) assigned to each predictor by the NCA corresponds to the relevance of each feature for the classification process. Higher weight indicates increased feature importance, while weight values converging to 0 represent redundant features for the particular classification problem (see Fig. 3). The weight threshold (θ_w) was determined as $\theta_w = T \cdot max(FW)$, where T = 0.4.

The advantages of NCA compared to the PSO and other relevant dimensionality reduction techniques are numerous, facilitating its easy implementation. To be exact, NCA proves particularly advantageous when combined with a kNN approach, maximizing classifier performance by forcing a low-rank linear transformation of the data [20]. Unlike other methods, this classification model is also non-parametric, meaning that it does not make any assumptions on the shape of the class distributions or the boundaries between them [21], while PSO requires a fine parameter selection and tuning before its implementation. Additionally, PSO remains vulnerable to prematurely converging and trapping into local minima, especially as problem dimensionality increases [22].

4) kNN Classification Strategy: The kNN classification algorithm has already demonstrated its potential for producing reliable and accurate predictions in previous works [10,11]. Its simplicity is a notable feature, employing straightforward comparisons for identifying similar records in the training data, thus proving effective in generating accurate predictions. In our implementation, we utilized the Euclidean distance between a test and a training data point, complemented by an inverse distance weight [23]. We selected k=9 nearest neighbors, while each predictor variable underwent centering and scaling based on their corresponding weighted column mean and standard deviation. A dedicated classifier was trained for each segmented window, resulting in a total

	W1	W2	W3	W4	W5	W6	SUM
LTA	1	3	7	5	4	2	22
LSOL	6	12	5	6	4	2	35
LGA	6	4	16	14	12	11	63
LVL	6	10	11	11	14	7	59
LVM	5	3	3	4	6	8	29
LRF	6	4	5	4	2	8	29
LBF	4	12	10	10	4	2	42
RTA	5	4	3	6	4	1	23
RSOL	2	6	6	3	4	2	23
RGA	4	3	8	4	1	4	24
RVL	3	3	4	4	3	3	20
RVM	2	3	8	3	5	2	23
RRF	6	10	7	8	6	3	40
RBF	6	8	3	5	2	3	27

TABLE II: Appearance frequency of the selected EMG features per muscle and per segmented window across subjects (i.e. 22 features of the LTA muscle appear in total across all subjects and windows meaning that 1 LTA feature was selected in Window 1, 3 LTA features in Window 2, 7 LTA features in Window 3, etc.)

of six separate classifiers and decisions per gait cycle. The input to each window classifier was the feature vector that emerged after the NCA feature selection as described in section II-D.3. The outlined approach for feature selection and classification yielded six distinct decisions for each of the six windows per gait cycle.

5) Final Decision via a Naive Bayes Implementation: To consolidate the distinct classifier decisions into a conclusive prediction about the stiffness $(S_R,\,S_H,\,S_M,\,{\rm or}\,\,S_L)$ of the upcoming surface, we employed a Naive Bayes classifier. Naive Bayes classification, rooted in Bayesian probability theory, is a probabilistic machine learning algorithm that is widely used within classification frameworks due to the advantages it offers with respect to its quick training times. The resulting kNN window classifiers analyzed previously were integrated into the training process of Naive Bayes, and the testing data initially used for assessing kNN classifiers were also used for evaluating the performance of the Naive Bayes.

III. RESULTS

Through the adoption of NCA as our feature selection method, we achieved a substantial average reduction of 91% in the number of selected classification input features, streamlining the initial count of 306 features per window to approximately 25 ± 5 . The significance of this feature reduction lies in minimizing the information channels utilized per experiment, thereby enhancing computational efficiency. On the contrary, employing PSO as our feature selection method, the number of the selected classification input features was reduced by 54 % on average, dropping the initial 306 features to approximately 142 ± 3 per window.

A meticulous examination of the frequency of feature appearance across windows and subjects can provide valuable

	W1	W2	W3	W4	W5	W6	SUM
LAF	5	3	3	5	3	4	23
LHF	2	1	4	1	3	0	11
LKF	0	2	0	4	1	2	9
RAF	2	1	2	3	1	3	12
RHF	3	3	3	2	1	2	14
RKF	2	2	2	2	2	1	11
CoM_x	1	2	1	1	2	4	11
CoM_y	5	3	1	4	4	6	23
CoM_z	2	3	3	3	3	2	16
RAV	2	3	3	4	2	2	16
LAV	1	3	2	2	4	1	13
RKV	2	4	1	0	3	2	12
LKV	2	2	5	5	2	1	17
RAA	0	2	5	4	11	5	27
LAA	6	4	5	2	2	6	25
RKA	3	4	3	4	3	2	19
LKA	1	4	4	2	1	2	14
GRF	2	5	2	1	2	3	15

TABLE III: Appearance frequency of the selected kinematic features per kinematic variable and per segmented window across subjects (i.e. 23 features of the Left Ankle Flexion (LAF) variable appear in total across all subjects and windows meaning that 5 LAF features were selected in Window 1, 3 LAF features in Window 2, 3 LAF features in Window 3, etc.)

insights into the essential information channels required for developing a robust and reliable high-level control framework for powered prostheses and wearable devices. Tables II and III present the appearance frequency of different EMG and kinematic feature variables per window across subjects, respectively. By focusing on the orange shaded values within the 'SUM' column in both tables, it becomes evident that they correspond to the most consistently selected variables across participants. For the case of the EMG features, the below-knee muscle LGA, along with the aboveknee muscles LVL, LVM, LBF, and RRF, emerge as the top five muscle variables chosen by NCA for achieving optimal prediction accuracy. Assuming that the leading (left) leg is the amputated limb, this finding substantiates the significance of hip extensors and flexors as major power contributors when ankle plantar flexor power is absent [24,25].

Turning to the kinematic features, the RAA and LAA followed by LAF and CoM_y , as well as RKA constitute the top five kinematic variables selected by NCA. The features corresponding to the ankle accelerations could indicate a modified step length as participants prepare to step on a new surface, while the ankle angle feature could be correlated with an increased toe clearance during such transitions. Overall, the kinematic features selected show potential for the non-leading leg to provide substantial information about user intent during transitions between compliant surfaces.

Although adding the GRF stand-alone values to each window vector does not seem to necessarily provide valuable

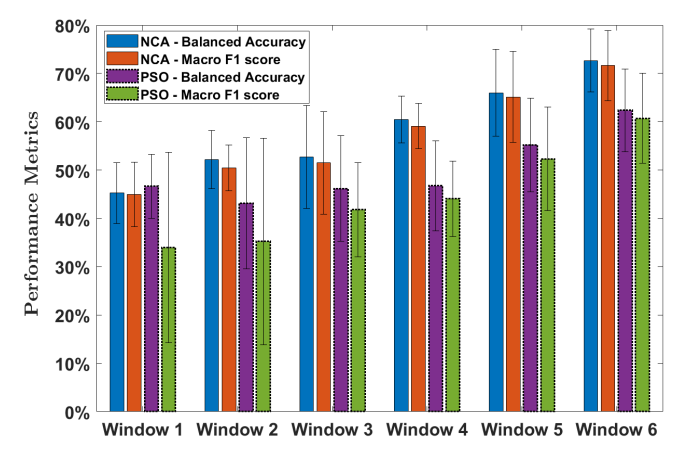


Fig. 4: Subject average performance evaluation metrics using kNN window classifiers with the NCA and PSO feature selection methods.

information as classification features, they are selected more frequently than other features, i.e., left knee or hip flexion. We hypothesize that the existence of GRF data from both feet could have provided us with better insights into their role in the classification process.

We can therefore safely deduce that out of the 14 EMGs initially recorded, we could have selected only 5 EMG electrodes, corresponding to the top 5 muscles as defined in Table II, while out of the 20 markers used to record the kinematics, we could have recorded the markers necessary to reproduce the top 5 kinematic variables as defined in Table III. This could lead to a drastic reduction in the number of sensors, improving the feasibility and the simplicity of the proposed framework.

In terms of classification accuracy, the performance analysis of each window classifier highlights a consistent trend of increased prediction accuracy as we approach the latter segments of each gait cycle for both the NCA and PSO input feature sets across subjects (see Fig. 4). The mean values for Balanced Accuracy and Macro F1 metrics show an ascending trend with increasing window numbers, reaching 72.67% and 71.6% for NCA and 62.36% and 60.69% for PSO, respectively for window 6. It becomes clear that NCA exceeds the performance of PSO for this multiclass problem throughout all of the classification windows, which justifies the final choice of NCA for our framework.

Incorporating the Naive Bayes classification as the final step in our framework improved the classification accuracy by 4.58%. Comparative evaluations with simple and weighted majority vote techniques demonstrated that the Naive Bayes approach outperformed these alternatives, though the differences were not statistically significant (Fig. 5). Notably, the weighted alternative of the simple majority vote showed slightly improved predictions, albeit without reaching statistical significance, as anticipated.

In addition to the drastic reduction of the used features, comparing our current work with our previous study, we observe an improved classification accuracy across subjects throughout all windows. The current study achieved a peak average kNN prediction accuracy of 72.67%, exceeding the

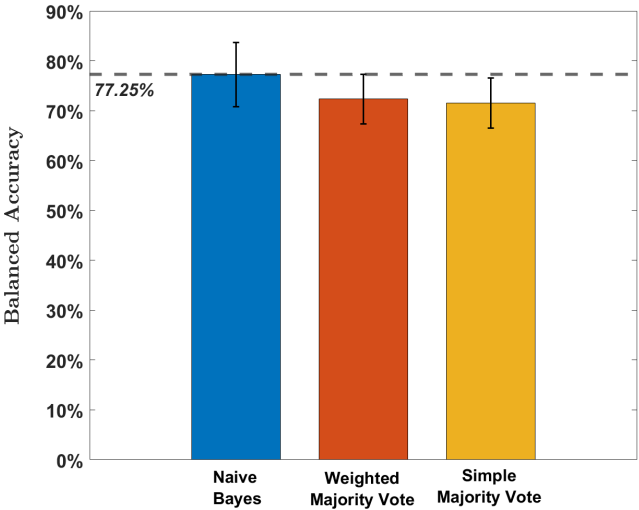


Fig. 5: Subject average performance evaluation metrics using k-NN window classifiers with the NCA and PSO feature selection methods

equivalent reached in [10] by 3.31%. Although 3.31% might not seem significant, we need to acknowledge the elevated challenge of this task, which includes four distinct classes instead of two as in our previous work.

IV. CONCLUSION

This paper investigates the selection and integration of EMG, kinematic, and GRF signals to streamline the predictive modeling process. Our goal is to harness the capabilities of the employed sensors while minimizing their number, creating a framework that accurately predicts user intent to transition to compliant surfaces.

The results of this work are particularly significant as the classification involves distinguishing between four classes, all associated with walking on a rigid surface. The developed framework holds potential for integration as part of a high-level controller, informing the prosthesis or lower extremity device and dynamically adjusting its parameters in real-time. Through this research, we aim to contribute to the ongoing efforts to improve the quality of life for individuals with lower limb amputations by making assistive technologies more accessible, efficient, and user-friendly.

REFERENCES

- B. J. Hafner, S. J. Morgan, D. C. Abrahamson, and D. Amtmann, "Characterizing mobility from the prosthetic limb user's perspective: Use of focus groups to guide development of the prosthetic limb users survey of mobility," *Prosthetics and Orthotics International*, vol. 40, pp. 582–590, 10 2016.
- [2] M. R. Tucker, J. Olivier, A. Pagel, H. Bleuler, M. Bouri, O. Lambercy, J. R. D. Millán, R. Riener, H. Vallery, and R. Gassert, "Control strategies for active lower extremity prosthetics and orthotics: A review," *Journal of NeuroEngineering and Rehabilitation*, vol. 12, pp. 1–30, 1 2015.
- [3] A. J. Young, T. A. Kuiken, and L. J. Hargrove, "Analysis of using emg and mechanical sensors to enhance intent recognition in powered lower limb prostheses," *Journal of Neural Engineering*, vol. 11, p. 056021, 9 2014.
- [4] R. Woodward, A. Simon, E. Seyforth, and L. Hargrove, "Real-time adaptation of an artificial neural network for transfemoral amputees using a powered prosthesis," *IEEE Transactions on Biomedical Engi*neering, vol. 69, pp. 1202–1211, 3 2022.

- [5] H. Huang, F. Zhang, L. J. Hargrove, Z. Dou, D. R. Rogers, and K. B. Englehart, "Continuous locomotion-mode identification for prosthetic legs based on neuromuscular mechanical fusion," *IEEE Transactions on Biomedical Engineering*, vol. 58, pp. 2867–2875, 10 2011.
- [6] M. Liu, F. Zhang, and H. H. Huang, "An adaptive classification strategy for reliable locomotion mode recognition," Sensors (Basel, Switzerland), vol. 17, 9 2017.
- [7] R. Murray, J. Mendez, L. Gabert, N. P. Fey, H. Liu, and T. Lenzi, "Ambulation mode classification of individuals with transfemoral amputation through a-mode sonomyography and convolutional neural networks," *Sensors*, vol. 22, p. 9350, 12 2022.
- [8] K. G. Rabe and N. P. Fey, "Evaluating electromyography and sonomyography sensor fusion to estimate lower-limb kinematics using gaussian process regression," *Frontiers in Robotics and AI*, vol. 9, p. 58, 3 2022.
- [9] M. Li, B. Zhong, E. Lobaton, and H. Huang, "Fusion of human gaze and machine vision for predicting intended locomotion mode," *IEEE Transactions on Neural Systems and Rehabilitation Engineering*, vol. 30, pp. 1103–1112, 2022.
- [10] C. Angelidou and P. Artemiadis, "On predicting transitions to compliant surfaces in human gait via neural and kinematic signals," IEEE Transactions on Neural Systems and Rehabilitation Engineering, vol. 31, pp. 2214–2223, 2023.
- [11] C. Angelidou and P. Artemiadis, "On intuitive control of ankle-foot prostheses: A sensor fusion-based algorithm for real-time prediction of transitions to compliant surfaces," 2023 IEEE/RSJ International Conference on Intelligent Robots and Systems (IROS), pp. 2122–2127, 10 2023.
- [12] A. Barkan, J. Skidmore, and P. Artemiadis, "Variable stiffness tread-mill (VST): A novel tool for the investigation of gait," *Proceedings IEEE International Conference on Robotics and Automation*, pp. 2838–2843, 9 2014.
- [13] J. Skidmore, A. Barkan, and P. Artemiadis, "Variable stiffness tread-mill (VST): System development, characterization, and preliminary experiments," *IEEE/ASME Transactions on Mechatronics*, vol. 20, 2015.
- [14] H. J. Hermens, B. Freriks, C. Disselhorst-Klug, and G. Rau, "Development of recommendations for semg sensors and sensor placement procedures," *Journal of electromyography and kinesiology*, vol. 10, pp. 361–374, 10 2000.
- [15] J. Skidmore, A. Barkan, and P. Artemiadis, "Investigation of contralateral leg response to unilateral stiffness perturbations using a novel device," in 2014 IEEE/RSJ International Conference on Intelligent Robots and Systems, 9 2014, pp. 2081–2086.
- [16] C. Karakasis and P. Artemiadis, "F-VESPA: A kinematic-based algorithm for real-time heel-strike detection during walking," *IEEE International Conference on Intelligent Robots and Systems*, pp. 5098–5103, 2021.
- [17] B. Hobbs and P. Artemiadis, "A systematic method for outlier detection in human gait data," in 2022 International Conference on Rehabilitation Robotics (ICORR), 2022.
- [18] I. S. Dhindsa, R. Agarwal, and H. S. Ryait, "Performance evaluation of various classifiers for predicting knee angle from electromyography signals," *Expert Systems*, vol. 36, p. e12381, 6 2019.
- [19] X. Jiang, C. Napier, B. Hannigan, J. J. Eng, and C. Menon, "Estimating vertical ground reaction force during walking using a single inertial sensor," *Sensors (Basel, Switzerland)*, vol. 20, pp. 1–13, 8 2020.
- [20] A. K. Agrawal and G. Chakraborty, "Neighborhood component analysis to leverage the class label information during feature selection to enhance the damage classification performance," *Structures*, vol. 57, p. 105174, 11 2023.
- [21] J. Goldberger, S. T. Roweis, G. E. Hinton, and R. Salakhutdinov, "Neighbourhood components analysis," in *Advances in Neural Infor*mation Processing Systems 17, 2004, pp. 513–520.
- [22] A. G. Gad, "Particle swarm optimization algorithm and its applications: A systematic review," *Archives of Computational Methods in Engineering* 2022 29:5, vol. 29, pp. 2531–2561, 4 2022.
- [23] G.-F. Fan, Y.-H. Guo, J.-M. Zheng, and W.-C. Hong, "Application of the weighted k-nearest neighbor algorithm for short-term load forecasting," 2019.
- [24] H. Sadeghi, P. Allard, and M. Duhaime, "Muscle power compensatory mechanisms in below-knee amputee gait," *American Journal of Phys*ical Medicine and Rehabilitation, vol. 80, pp. 25–32, 1 2001.
- [25] C. L. Brockett and G. J. Chapman, "Biomechanics of the ankle," Orthopaedics and trauma, vol. 30, pp. 232–238, 6 2016.